Vibrational phase contrast CARS microscopy for quantitative analysis

M. Jurna[a], E.T. Garbacik[a], J.P. Korterik[a], C. Otto[b], J.L. Herek[a], H.L. Offerhaus[a]

[a] Optical Sciences group, [b] BioPhysical Engineering group, MESA+ Research Institute, Department of Science and Technology (TNW), University of Twente, The Netherlands.

ABSTRACT

In biological samples the resonant CARS signal of less abundant constituents can be overwhelmed by the non-resonant background, preventing detection of those molecules. We demonstrate a method to obtain the phase of the oscillators in the focal volume that allows discrimination of those hidden molecules. The phase is measured with respect to the local excitation fields using a cascaded phase-preserving chain. It is measured point-by-point and takes into account refractive index changes in the sample, phase curvature over the field-of-view and interferometric instabilities. The detection of the phase of the vibrational motion can be regarded as a vibrational extension of the linear (refractive index) phase contrast microscopy introduced by Zernike around 1933.

Keywords: Nonlinear optics, coherent anti-Stokes Raman scattering, spectroscopy, microscopy, heterodyne, phase detection, phase contrast

1. INTRODUCTION

Over the last decade CARS (coherent anti-Stokes scattering) microscopy has developed into a powerful imaging tool for studying biological questions in a non-invasive way.[1,2] CARS probes the vibrational modes of molecules, as in Raman imaging, to visualize a specific type of molecules within the sample. Coincidence between the difference frequency of the pump and Stokes input wavelengths with a vibrational mode, resonantly enhances the CARS (anti-Stokes) output signal.[3] CARS signal is also created non-resonantly. Depending on the ratio of resonant to non-resonant molecules in the focal volume, this non-resonant signal can overwhelm a small resonant signal. Samples that contain a lot of water, such as cells, give rise to a significant non-resonant signal, observed as a background over the full image. The intensity differences in such images are not based on chemical selectivity alone, but contain interferences between the resonant and non-resonant signal. Spontaneous Raman imaging lacks on coherent addition of the resonant signal yielding an acquisition speed that is applicable slow biological processes. The intensity of the CARS signal can be written as:

$$I_{CARS}(\omega) \propto \left|\chi_R^{(3)}(\omega) + \chi_{NR}^{(3)}\right|^2, \tag{1}$$

where the connection between Raman and CARS is given by:

$$I_{Raman}(\omega) \propto Im\left[\chi_R^{(3)}(\omega)\right]. \tag{2}$$

One commonly used method to remove the background is epi-CARS,[4] where the CARS signal is detected in the backward direction. This method does not offer discrimination between resonant and non-resonant CARS signal, but between large and small objects in the focal volume, based on phase matching. Small resonant objects give rise to CARS signal in both the forward and backward direction, whereas the surrounding bulk medium (e.g. non-resonant water) causes only CARS signal in the forward direction. Polarization CARS[5–7] truly removes the non-resonant signal, but often also rejects a large part of the resonant signal. Time-resolved CARS[8] rejects the non-resonant component by delaying the probe beam to exploit the differences in decay. Stimulated Raman scattering is inherently background free. It requires the detection of a small modulation on a large background but has been demonstrated successfully for imaging.[9,10] Dual pump CARS[11] measures the

Send correspondence to H.L. Offerhaus E-mail: H.L.Offerhaus@TNW.Utwente.nl

Multiphoton Microscopy in the Biomedical Sciences X, edited by Ammasi Periasamy, Peter T. C. So, Karsten König, Proc. of SPIE Vol. 7569, 75690F · © 2010 SPIE · CCC code: 1605-7422/10/$18 · doi: 10.1117/12.840178

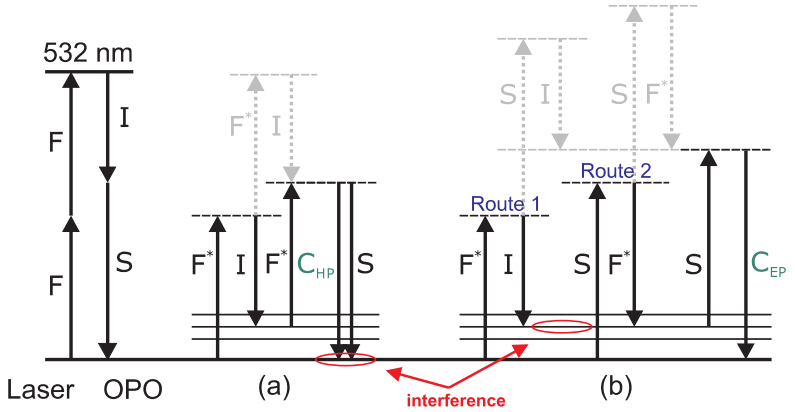

Figure 1. Schematic of cascaded phase-preserving chain between laser, OPO and CARS process. Where (a) shows the heterodyne phase detection scheme and (b) shows the local excitation phase detection scheme. F = fundamental laser (1064 nm), F* = modulated fundamental laser, I = idler OPO, S = signal OPO and C = CARS signal. In black and gray are respectively the resonant and non-resonant CARS process given.

non-resonant background separately, requiring an extra laser input, long integration times and high stability. Frequency Modulation (FM)CARS[12] uses the mixing between the resonant and non-resonant signal to detect the amplitude modulation. It requires less integration time and can reject the non-resonant background, but requires a constant non-resonant background for faithful reproduction of the resonant amplitude. Interferometric CARS[13] achieves rejection of the non-resonant CARS signal, without rejection of resonant signal by direct detection of the amplitude and phase of the CARS signal. The CARS signal is mixed with a stable external reference signal to avoid misinterpretation due to inhomogeneous distribution of the non-resonant background. In this paper we employ a cascaded phase-preserving chain to obtain the necessary stable reference signal for interferometric CARS detection without the need for extra lasers. We demonstrate detection of the phase of the CARS signal and detection of the phase of the excitation fields. Subtraction of those two yields the phase of the motion of the molecules with respect to the excitation fields, taking into account the changes in refractive index in the sample, the curvature of the field-of-view and any other phase disturbances in the sample. This clean phase provides a clean rejection of the non-resonant background and reveals the hidden detail to an arbitrary precision, limited only by imaging speed. This is the first demonstration of the detection of the phase with respect to the excitation fields and the only technique that offers shot noise limited performance and precision that is limited by integration time only. Phase contrast microscopy as introduced by Zernike[14] provided a new level of detail in samples that offered insufficient contrast in the transmission amplitude. Now, some 75 years later, the vibrational phase can be used to reject the non-resonant amplitude and improve the vibrational contrast.

2. DETECTION OF THE LOCAL EXCITATION PHASE

Interferometric detection mixes a reference field, the so-called local oscillator (LO) field, with the generated CARS field. This local oscillator must be phase- and wavelength-locked to the generated CARS signal. It has been shown previously that the local oscillator can be created in bulk media,[13,15] using a cascaded phase-preserving chain[16] or by using a Polarization CARS scheme.[17] Non of these schemes correct for the refractive index changes in the sample or amplitude mixing. In the cascaded phase-preserving chain an Optical Parametric Oscillator (OPO) is synchronously pumped by the second harmonic of a laser source. The CARS signal is generated with the fundamental of the laser source and the idler from the OPO. The signal from the OPO is phase- and wavelength-locked to the generated CARS signal and can therefore be used as the local oscillator, see Fig. 1(a).

The total intensity on the detector can be written as:

$$I_{detector} = |E_{LO}|^2 + |E_{AS}|^2 + 2E_{LO}E_{Ex} \cdot P \tag{3}$$

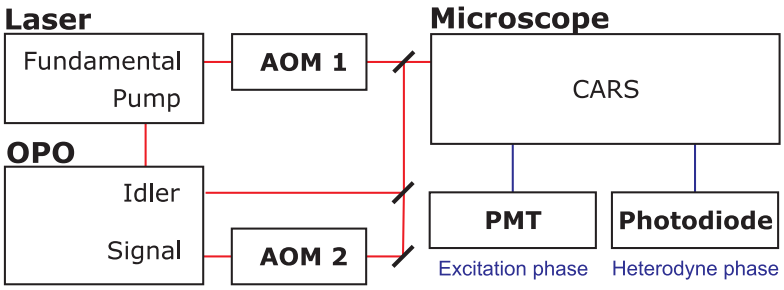

Figure 2. Schematic of the setup, where AOM 1 is phase modulated and AOM 2 is amplitude modulated

Where the CARS field $E_{AS} \propto E_{Ex}\left[\chi_R^{(3)} + \chi_{NR}^{(3)}\right]$, the excitation field $E_{Ex} = E_{Pump}^2 E_{Stokes}$ and P can be expressed as:

$$P = \left\{\left[\chi_{NR}^{(3)} + Re(\chi_R^{(3)})\right] cos\phi_\chi + \left[Im(\chi_R^{(3)})\right] sin\phi_\chi\right\}, \tag{4}$$

where ϕ_χ (vibrational phase response) is the phase difference between the total CARS field and the excitation field. This is the phase difference that distinguishes between the real (non-resonant) and the imaginary (resonant, Raman) part.[18] However, this is not directly the phase measured in the focal volume; even for co-propagating fields this phase is disturbed by refractive index changes in the sample, curvature of the field-of-view and interferometric instabilities. Detection of the local excitation phase and using this 'base' phase to correct the heterodyne detected phase gives the accurate phase of the oscillators in the focal volume, further referred to as 'vibrational phase'. For our cascaded chain (figure 1a), the phase difference (Δ_1), obtained by the interference between the local oscillator (the OPO signal beam) and the CARS signal (C_{HP}) is given by:

$$\begin{aligned} \Delta_1 &= \phi_S - \phi_{C_{HP}} \\ &= \phi_S - (2\phi_{F^*} - \phi_I + \phi_\chi) \\ &= 2\phi_F - 2\phi_{F^*} - \phi_\chi, \end{aligned} \tag{5}$$

where F^* is a frequency shifted version of F. Figure 1(b) shows the detection of the local excitation phase, where there are two separate routes to the same vibrational level (or continuum level) creating an interference that can be probed by the OPO signal and detected at the C_{EP} wavelength, given by $2S - F^*$. The interference arises from the phase difference between the two pathways (Δ_2):

$$\begin{aligned} \Delta_2 &= Route\ 2 - Route\ 1 \\ &= (\phi_S - \phi_{F^*}) - (\phi_{F^*} - \phi_I) \\ &= 2\phi_F - 2\phi_{F^*}. \end{aligned} \tag{6}$$

The difference between the Δ_2 and Δ_1 is now purely due to the interaction with the vibrational phase response ϕ_χ.

$$\begin{aligned} Vibrational\ phase &= \Delta_2 - \Delta_1 \\ &= (2\phi_F - 2\phi_{F^*}) - (2\phi_F - 2\phi_{F^*} - \phi_\chi) \\ &= \phi_\chi. \end{aligned} \tag{7}$$

Phase disturbances will occur within the acquisition time of one frame and over the full field-of-view. Detection on a alternated phase detection on a point-by-point basis over the sample overcomes these interferometric instabilities.

3. DETECTION SETUP

The key elements of the setup (see figure 2) are the laser source, a Nd:YAG laser (Coherent Paladin, 1064 nm and 532 nm), and a synchronously pumped OPO (APE Levante Emerald). This combination provides a

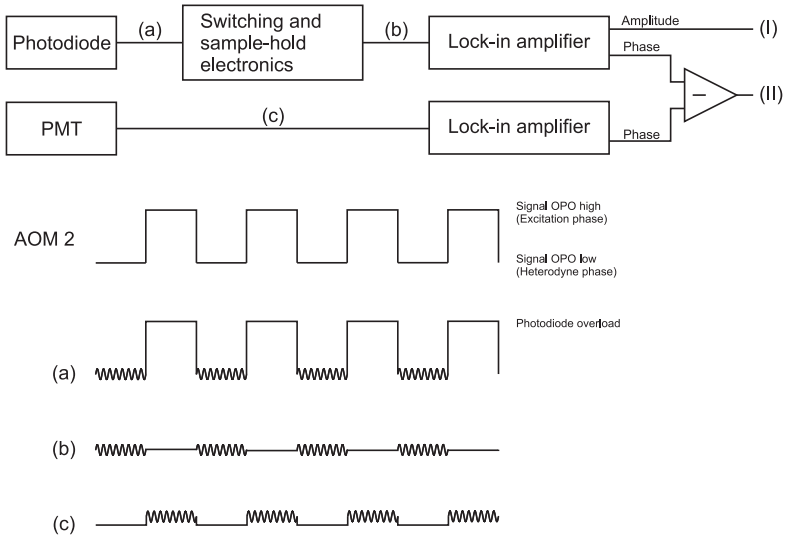

Figure 3. Electronical signal processing scheme to obtain the vibrational amplitude and phase. The output signals (I) and (II) are respectivily the vibrational amplitude and phase. AOM 2 shows the switching of the signal of the OPO, (a) detected Photodiode signal, (b) Photodiode signal after switching and sample-hold electronics and (c) PMT signal.

well-controlled and stable local oscillator.[19] The input powers of the fundamental and idler are several tens of mW, the power of the local oscillator is only a few nW. Heterodyne interferometric detection is obtained by shifting the CARS frequency by an acousto-optical modulator (AOM 1, first order) in the fundamental branch. By detecting the laser repetition rate and using a voltage controlled oscillator (VCO), an external frequency of 50 kHz is added to the detected laser repetition rate and applied to the acousto-optical modulator. This 50 kHz shift is translated to a 100 kHz shift at the CARS wavelength (two photons in the CARS process). The CARS signal is detected on a photodiode (shot noise limited[16]) and fed to a lock-in amplifier (Stanford Research SR830) set to detect at 100 kHz.

For detection of the local excitation phase (figure 1b), the amplitude of the signal of the OPO is now changed from a few nW to the same level as the fundamental beam to balance the contribution of both pathways, route 1 and route 2. The result of both routes is probed by the signal of the OPO and detected on a PMT (or Photodiode).

To overcome interferometric instabilities between the two phase detection methods, an alternated phase detection on a point-by-point basis is added to the setup. Switching between the two power levels is done by a second acousto-optical modulator (AOM 2) in the OPO signal branch. This acousto-optical modulator is also used in first order (to obtain the necessary high extinction ratio), but driven at the laser repetition rate to prevent frequency modulation. The amplitude modulation ($\sim$1 kHz) of AOM 2 is set to a multiple of the galvano scanners in the microscope. Scanning at 1 ms/pixel, results in alternating detection between the two different phase detection schemes. First the heterodyne phase is detected on the photodiode, when AOM 2 passes only a few nW, and second the local excitation phase is detected on the PMT, when AOM 2 passes all OPO-signal power, see figure 3. By switching and sample-hold electronics the overload during the excitation phase detection time on the photodiode is removed. The detection of the local excitation phase is done by a second lock-in amplifier at the same 100 kHz modulation. Both lock-in amplifiers are set to 1 ms integration time. Shorter pixel dwell times can be obtained by higher external modulation frequencies and shorter integration times.

A demonstration of the vibrational phase detection is shown in figure 4, where a sample fat spheres (mayonaise) of different sizes distributed in agarose gel is imaged. The phase of the heterodyne signal contains the vibrational phase of the sample, but the vibrational phase is hard to distinguish (due to the refractive index changes in the sample, phase curvature over the field of view and interferometric instabilities). The excitation

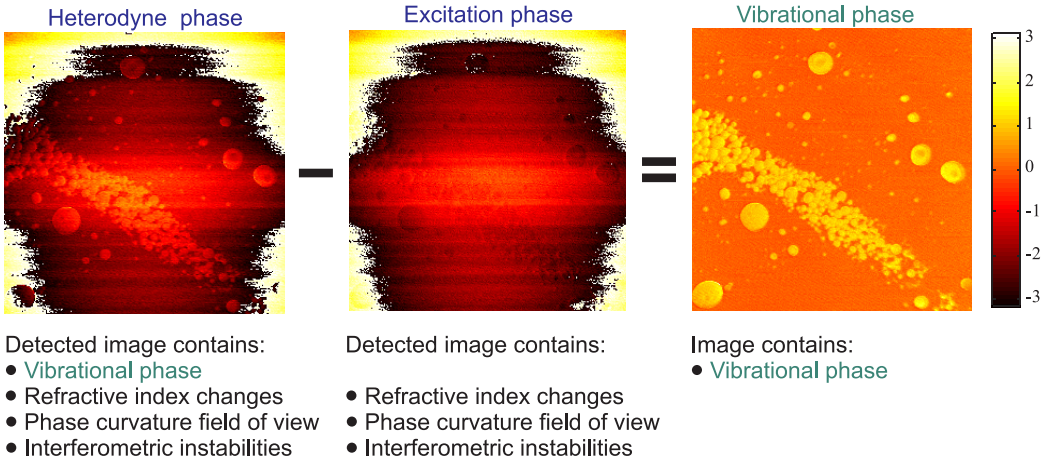

Figure 4. A sample of fat spheres (mayonaise) of different sizes distributed in a agarose gel sollution imaged at 2865 cm^{-1}. The subtraction of the heterodyne phase from the excitation phase shows a clear vibrational phase, without phase disturbances of the refractive index, curvature of field-of-view and interferometric instabilities.

phase shows also the phase disturbances, but not the vibrational phase. The subtraction of the excitation from the heterodyne phase yields the vibrational phase of the sample, without disturbances. In the vibrational phase image, phase steps can be seen on the location of the fat spheres. The non-resonant agarose gel show a flat phase.

4. IMAGING OF HELA CELLS

To demonstrate the capability of the phase detection scheme, further referred to as "Vibrational Phase Contrast CARS" or VPC-CARS,[20] HeLa cells are imaged. Figure 5 shows fixed HeLa cells in water that contain lipid droplets of various sizes. CARS images of 50x50 μm, 262x262 pixels taken with a 1.2 NA water objective are acquired at 2845 cm^{-1}. The heterodyne phase, figure 5(a), shows that the phase over the field-of-view is not constant, but distorted and noisy. At the location of the lipids in the cell we can see phase steps. These phase steps are mostly due to the difference in phase between resonant and non-resonant signal. Figure 5(b) shows the local excitation phase detected on the PMT which is also distorted and noisy. Again phase steps are observed at the location of the lipid droplets but these phase steps are caused by the difference in refractive index between lipid and the water in the cell. The amplitude image of the CARS signal is shown in figure 5(c). There is contrast between the cells and the surrounding water and the internal structure within the cells can be observed despite the lack of resonant material there. Resonant lipid droplets can easily be seen, as the amplitude of many droplets exceeds the non-resonant signal. Interferences on the edges of the droplets yield a 'dark' ring around the droplets, enhancing the contrast. Note that there are also droplets represented by dark spots in the amplitude image. Subtraction of the local excitation phase from the oscillator phase can be seen in figure 5(d). The distortion and noise are canceled, allowing for averaging of this vibrational phase image to increase the precision on the phase value. In this image the phase of the pure non-resonant water signal outside the cell is used to pinpoint phase zero and subtract a residual phase difference that is caused by the AOM switching between different levels. Since there is a strong non-resonant background, the phase step at the lipids does not reach $\pi/2$, see figure 5(f), line cross section (d). Equation 4 shows that taking the sine of the vibrational phase image and multiplying it with the amplitude image, removes the non-resonant signal, which is done in figure 5(e). Comparing the amplitude image and the background free image, it can be seen that the internal structure of the cell and the edge of the cell have disappeared and only the resonant lipids can be observed. This shows that the cell structure in the amplitude image is non-resonant and should not be confused for the resonant material at the cell boundary. The line cross section, see figure 5(f), shows that the non-resonant amplitude is lowered from 0.25 to less than 0.02. The three lipid droplets in the line cross section around 42 μm show only a small drop in amplitude due to the $\sim \pi/4$ phase step at these locations. The region between 0 and 15 μm shows lipid droplets that are faint compared to the non-resonant signal, but stand out when the non-resonant signal is removed. The dispersive feature at

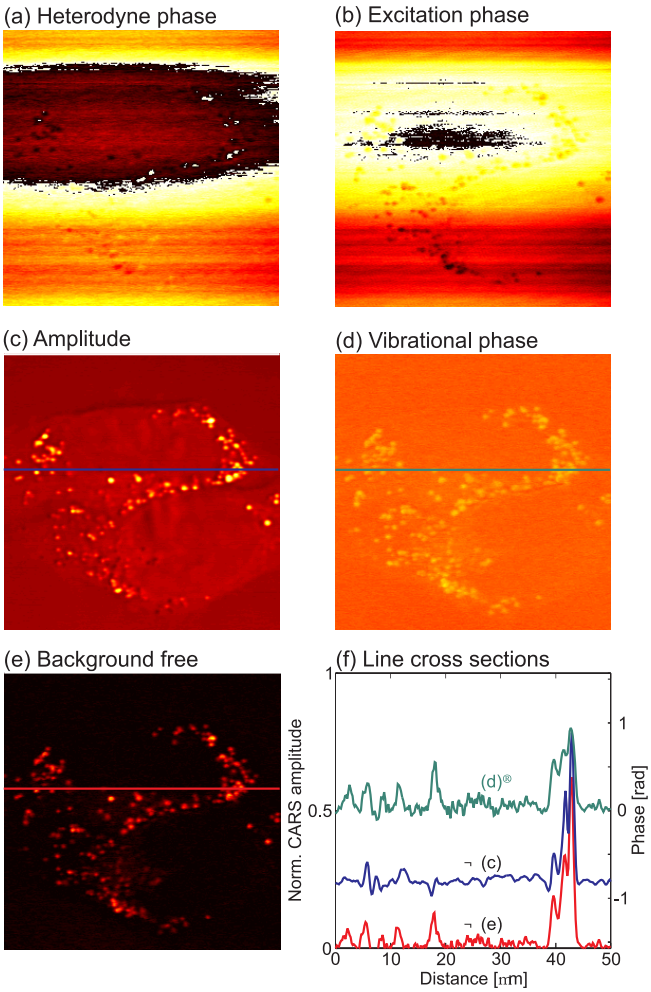

Figure 5. Fixed HeLa cells in water with various sizes of lipid droplets imaged at the vibrational stretch of 2845 cm^{-1}. (a-b) are respectively heterodyne phase and local excitation phase images. (c-d) are respectively five times averaged CARS amplitude and vibrational phase image (subtraction of the local excitation phase from the oscillator phase). (e) Background free amplitude. (f) Line cross sections of images c, d and e. The scaling of the phase images (a, b and d) are the same. The scaling of the amplitude images (c and e) are also the same.

18 μm, is also accompanied by a phase step, resulting in a recovered clean amplitude in the background free image.

5. MULTI COMPOUND ANALYSIS

Every specific molecule has an amplitude and phase, that depend on the driving frequency. The amplitude and phase represent a vector length and angle in the complex plane. A single resonance traces a circle in the complex plane as a function of frequency. Multiple resonances result in a circle with additional circular features. Extending this complex plane with a third axis for the driving frequency of the molecule, a spiral or corkscrew in complex space can be constructed, see figure 6. Looking along the frequency axis (front view) shows the complex plane. When we look along the the imaginary-axis (bottom view) we obtain the real plane. This plane shows the typical dispersion caused by wavelength depended refractive index changes. The last view in this 3D plane is along the real-axis (side view) and gives the imaginary-plane. This view gives the absorption profile of the molecule and is directly related to the Raman intensity spectrum of the molecule (equation 2). With this insight of the vibrational stretches of molecules in the complex 3D plane, it becomes clear that some resonances seem

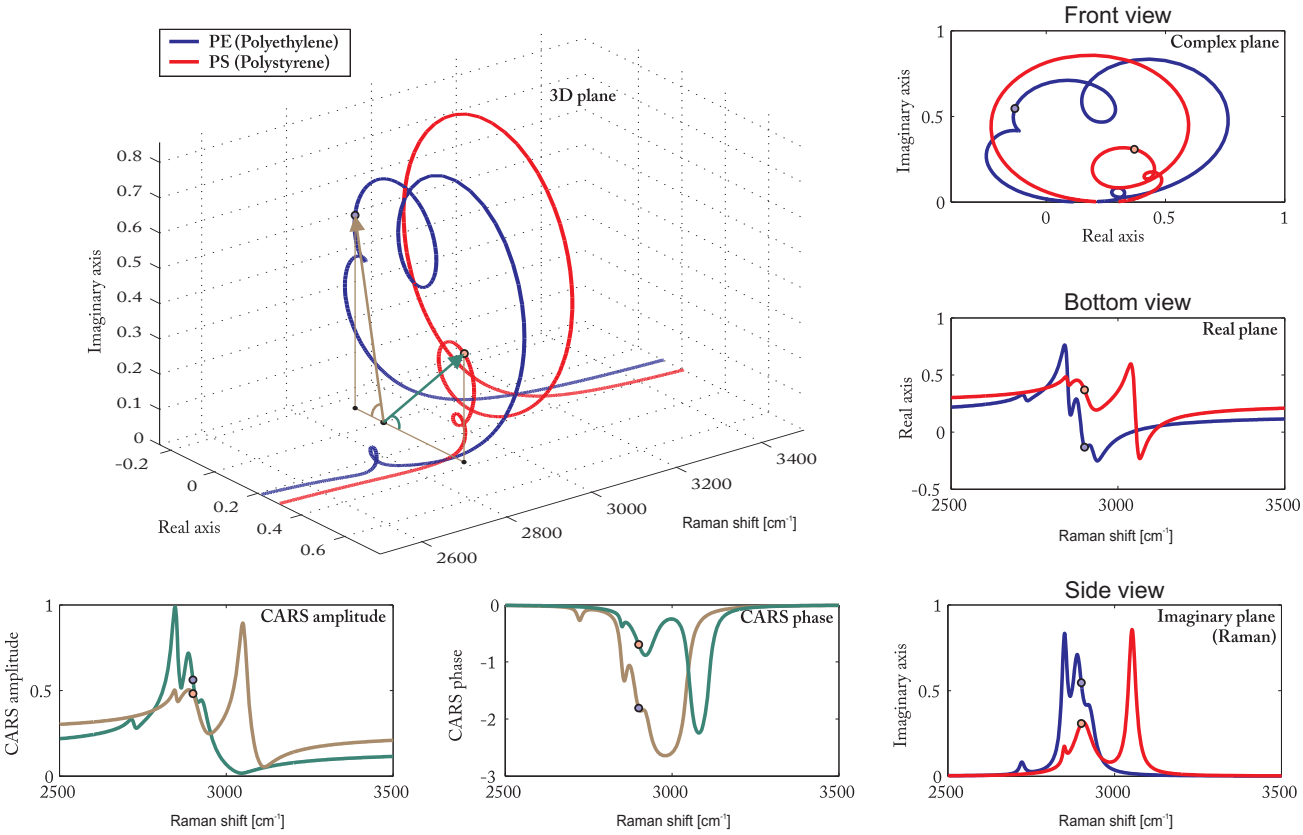

Figure 6. The resonances of PMMA and PS where the position in the complex plane is plotted against the frequency. The three different views of this 3D plane are on the right side and underneath are the amplitude and phase given of the CARS signal.

to be overlapping in the CARS amplitude spectrum, but have a significant difference in phase.

The 3D picture can be used when different materials have overlapping resonances and selectivity based on amplitude separation is not possible. In figure 7, a combination of three different materials is imaged with VPC-CARS at a single vibrational frequency. The sample contains a Polyethylene (PE) sheet on the left side, 4 μm PMMA beads and water. The amplitudes of the PE and PMMA are the same and the signal from the water is so weak that it can be considered non-resonant background signal. In the phase image a clear difference can be observed between the PE and PMMA. When all points in the image (amplitude and phase information) are plotted in a density complex plane plot, it is possible to distinguish four different areas. The points in these four different areas can be plotted separately to show the pure constituents and one mix image. These images are all free from background signal. This shows that VPC-CARS allows for multi component separation imaging at a single vibrational stretch.

6. CONCLUSION

We demonstrated a cascaded phase-preserving chain to obtain the phase of oscillating molecules with respect to the excitation field for background free imaging. Two phase detection schemes are alternated on a point-by-point base, so that the acquired phase is corrected for refractive index changes in the sample, phase curvature over the field-of-view and interferometric instabilities. The phase detection improves the signal-to-background by an order of magnitude allowing for imaging of concentrations ten times lower than previously attainable. Furthermore we showed the possibility of multi component analysis based on the complex information.

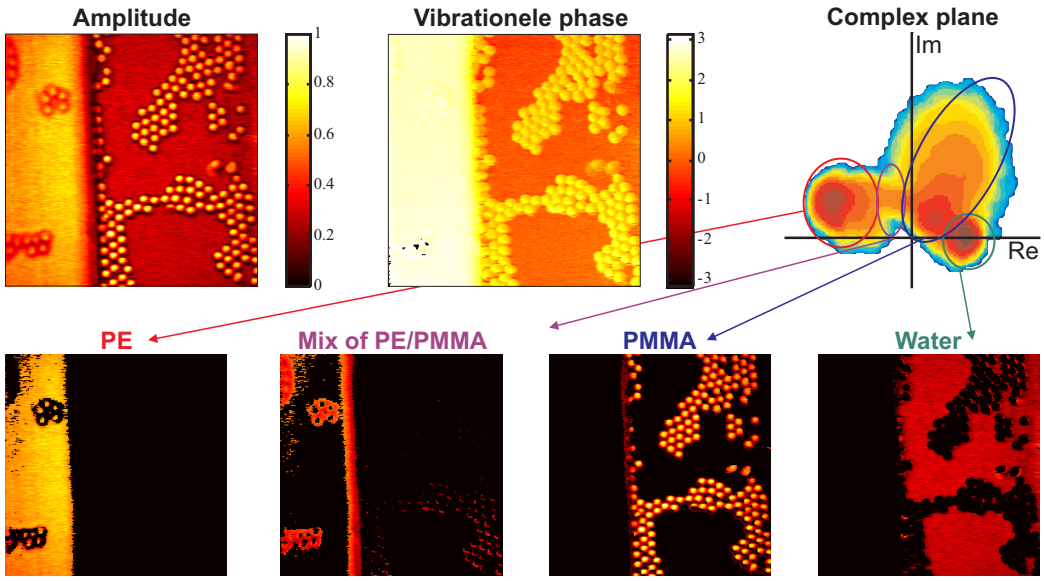

Figure 7. Multi component analysis of a sample containing a sheet of PE (left), 4 μm PMMA beads and water imaged at 2940 cm^{-1}. The different compounds can be separated by its location in the complex plane.

ACKNOWLEDGMENTS

This research is supported by NanoNed, a nanotechnology programme of the Dutch Ministry of Economic Affairs and partly financed by the Stichting voor Fundamenteel Onderzoek der Materie (FOM), which is financially supported by the Nederlandse Organisatie voor Wetenschappelijk Onderzoek (NWO). We also acknowledge Coherent Inc. for the use of the Paladin laser and APE Berlin for the collaboration and use of a Levante Emerald OPO.

REFERENCES

[1] Hellerer, T., Axaeng, C., Brackmann, C., Hillertz, P., Pilon, M., and Enejder, A., "Monitoring of lipid storage in caenorhabditis elegans using coherent anti-stokes raman scattering (cars) microscopy," *Proc. Natl. Acad. Sci. U. S. A.* **104**, 14658–14663 (SEP 11 2007).

[2] Nan, X., Potma, E., and Xie, X., "Nonperturbative chemical imaging of organelle transport in living cells with coherent anti-stokes raman scattering microscopy," *Biophys. J.* **91**, 728–735 (JUL 15 2006).

[3] Muller, M. and Zumbusch, A., "Coherent anti-stokes raman scattering microscopy," *ChemPhysChem* **8**, 2157–2170 (OCT 22 2007).

[4] Volkmer, A., Cheng, J., and Xie, X., "Vibrational imaging with high sensitivity via epidetected coherent anti-stokes raman scattering microscopy," *Phys. Rev. Lett.* **87**, 023901 (JUL 9 2001).

[5] Akhmanov, S., Bunkin, A., Ivanov, S., and Koroteev, N., "Polarization active raman spectroscopy and coherent raman ellipsometry," *Sov.Phys. JETP* **47**, 667 (1978).

[6] Chikishev, A., Lucassen, G., Koroteev, N., Otto, C., and Greve, J., "Polarization sensitive coherent anti-stokes-raman scattering spectroscopy of the amide i band of proteins in solutions," *Biophys. J.* **63**(4), 976–985 (1992).

[7] Cheng, J., Book, L., and Xie, X., "Polarization coherent anti-stokes raman scattering microscopy," *Opt. Lett.* **26**, 1341–1343 (SEP 1 2001).

[8] Volkmer, A., Book, L., and Xie, X., "Time-resolved coherent anti-stokes raman scattering microscopy: Imaging based on raman free induction decay," *Appl. Phys. Lett.* **80**, 1505 (2002).

[9] Freudiger, C. W., Min, W., Saar, B. G., Lu, S., Holtom, G. R., He, C., Tsai, J. C., Kang, J. X., and Xie, X. S., "Label-free biomedical imaging with high sensitivity by stimulated raman scattering microscopy," *Science* **322**, 1857–1861 (DEC 19 2008).

[10] Nandakumar, P., Kovalev, A., and Volkmer, A., "Vibrational imaging based on stimulated raman scattering microscopy," *New J. Phys.* **11**, 033026 (MAR 25 2009).

[11] Burkacky, O., Zumbusch, A., Brackmann, C., and Enejder, A., "Dual-pump coherent anti-stokes-raman scattering microscopy," *Opt. Lett* **31**, 3656–3658 (DEC 15 2006).

[12] Ganikhanov, F., Evans, C., Saar, B., and Xie, X., "High-sensitivity vibrational imaging with frequency modulation coherent anti-stokes raman scattering (fm cars) microscopy," *Opt. Lett.* **31**(12), 1872–1874 (2006).

[13] Potma, E., Evans, C., and Xie, X., "Heterodyne coherent anti-stokes raman scattering (cars) imaging," *Opt. Lett.* **31**, 241–243 (JAN 15 2006).

[14] Zernike, F., "Phase-contrast, a new method for microscopic observation of transparent objects," *Physica* **9**, 686–698 and 974–986 (1942).

[15] Andresen, E., Keiding, S., and Potma, E., "Picosecond anti-stokes generation in a photonic-crystal fiber for interferometric cars microscopy," *Opt. Express* **14**, 7246–7251 (AUG 7 2006).

[16] Jurna, M., Korterik, J. P., Otto, C., and Offerhaus, H. L., "Shot noise limited heterodyne detection of cars signals," *Opt. Express* **15**, 15207–15213 (NOV 12 2007).

[17] Lu, F., Zheng, W., and Huang, Z., "Heterodyne polarization coherent anti-stokes raman scattering microscopy," *Appl. Phys. Lett.* **92**, 123901 (MAR 24 2008).

[18] Jurna, M., Korterik, J. P., Otto, C., Herek, J. L., and Offerhaus, H. L., "Background free cars imaging by phase sensitive heterodyne cars," *Opt. Express* **16**, 15863–15869 (SEP 29 2008).

[19] Jurna, M., Buttner, E., Korterik, J., Otto, C., Rimke, I., and Offerhaus, H., "Shot noise limited heterodyne detection of cars signals," *Proc. SPIE* **6860**, 68600R (2008).

[20] Jurna, M., Korterik, J. P., Otto, C., Herek, J. L., and Offerhaus, H. L., "Vibrational phase contrast microscopy by use of coherent anti-stokes raman scattering," *Phys. Rev. Lett.* **103**(4), 043905 (2009).